ISSN 0023-1584, Kinetics and Catalysis, 2010, Vol. 51, No. 6, pp. 823–827. © Pleiades Publishing, Ltd., 2010.

VIII INTERNATIONAL CONFERENCE
ON MECHANISMS OF CATALYTIC REACTIONS

CO Oxidation over $Au/CeO_2–ZrO_2$ Catalists: The Effect of the Support Composition of the Au-Support Interaction[1]

I. Dobrosz-Gómez[a,b], M. Á. Gómez-García[b], and J. M. Rynkowski[a]

[a] *Technical University of Łódź, Poland*

[b] *Universidad Nacional de Colombia, Manizales, Colombia*

e-mail: jacryn@p.lodz.p

Received September 30, 2009

Abstract—The effect of the support composition on the Au-support interactions and its role in the creation of the activity of $Au/CeO_2–ZrO_2$ catalysts in CO oxidation has been studied. The $CeO_2–ZrO_2$ oxides and $Au/CeO_2–ZrO_2$ catalysts were synthesized, characterized by BET, XRD, HRTEM, AAS, TPR-H_2, and tested in CO oxidation. An approximate evaluation of the H_2 consumption for the surface reduction of the studied samples was estimated applying the model developed by Johnson and Mooi, which is based on the qualitative relationship between the amount of the capping oxygen and BET surface area. The sequence of the increasing percentage of O_2 atoms in the capping peak to the total Ce atoms follows the sequence of the decreasing Zr/Ce molar ratio in the sample. The activity of $Au/CeO_2–ZrO_2$ catalysts depends on the support composition and increases with the decrease in Zr/Ce molar ratio.

DOI: 10.1134/S0023158410060078

Cold-start emissions are responsible for ~80% of the pollution emitted by gasoline vehicles, since conventional three way catalysts are not efficient at temperatures below 200°C [1]. Carbon monoxide is one of the main pollutants emitted during the cold-start operation. In order to comply with the new limits imposed by the legislation on pollution control, more efficient catalysts are required. Since the discovery of the high activity exhibited by supported gold particles (3–5 nm) in CO oxidation at low temperature, the interest in using Au as a catalyst component has increased enormously [2–5]. Beside the role of Au particle size, the importance of the oxide support, not only as a stabilizer of the Au dispersion or modifier of the Au electronic state, but also as a participant in activation of reactants, especially oxygen, is considered [6–8]. Moreover, several other interactions can also occur at the metal-oxide interface, resulting in substantial modifications of the physicochemical and catalytic properties of both the oxide and the metal. Many questions concerning especially interactions at the metal-support interface, resulting in substantial modifications of the physicochemical and catalytic properties of both the support and the metal, remain still not clear. Previously, we reported the usefulness of $Ce_{1-x}Zr_xO_2$ (x = 0, 0.25, 0.5, 0.75, 1) oxides as supports for Au nanoparticles, mainly from the point of view of their contribution to the reaction [9], and different factors influencing the structure and catalytic activity of $Au/Ce_{1-x}Zr_xO_2$ catalysts in CO oxidation [10, 11]. Ceria-zirconia supported Au catalysts appeared to be very promising catalysts in CO oxidation [9, 10]. Furthermore, the significant influences of gold particle size on the Au-support interactions and on the activity of $Au/Ce_{0.75}Zr_{0.25}O_2$ in CO oxidation were observed [12].

Consequently, the aim of this work is to obtain a more detailed insight into the effect of the support composition on the Au-support interactions and its role in the creation of the activity of $Au/CeO_2–ZrO_2$ catalysts in CO oxidation. The $Ce_{1-x}Zr_xO_2$ (x = 0.25, 0.5, 0.75) oxides and $Au/CeO_2–ZrO_2$ catalysts were synthesized, characterized by BET, AAS, HRTEM, XRD, TPR-H_2, and tested in CO oxidation under stationary conditions. Moreover, an approximate evaluation of the H_2 consumption for the surface reduction of the studied samples was estimated applying the model developed by Johnson and Mooi [13], based on the qualitative relationship between the magnitude of the capping oxygen and BET surface area.

EXPERIMENTAL

Synthesis

A series of $Ce_{1-x}Zr_xO_2$ (x = 0.25, 0.5, 0.75) solid solutions, used as supports for Au, was prepared by the sol-gel like method, based on a thermal decomposition of mixed propionates [9]. Cerium(III) acetyloacetonatehydrate $Ce(CH_3COCH_2COCH_3)_3 \cdot H_2O$ (Sigma-

[1] The article is published in the original.

Aldrich, purity 99.9%) and zirconium(IV) acetylacetonate $Zr(CH_3COCH_2COCH_3)_4$ (Avocado, purity 99.9%), used as the starting materials, were dissolved in boiling propionic acid in concentration of 0.12 mol/l. As a result the propionate precursors were formed. Next, boiling solutions were mixed and the solvent was evaporated until a resin was obtained. Finally, all samples were calcined in air at 550°C for 4 h. Hydrogen tetrachloroaureate(III) trihydrate $HAuCl_4 \cdot 3H_2O$ (Sigma-Aldrich, purity 99.9%) was used as a gold precursor. The catalysts were prepared by the direct anionic exchange (method of gold species with hydroxyl groups of the support [4, 9, 14]. The optimization of catalyst synthesis conditions was presented previously [15]. Aqueous solutions of $HAuCl_4$ at the concentration 2.25×10^{-4} mol/l were prepared using 900 cm^3 of distilled water. The solution was heated up to 70°C and the support was introduced. After 1 h of thermostating and vigorous stirring, the suspension was centrifuged. In order to remove the residual chlorine from the catalysts, the obtained solid was suspended in 4 M ammonia solution, stirred for 1 h and next centrifuged again. After drying in an oven at 120°C overnight, the samples were calcined in air at 300°C for 4 h.

Characterization Methods

The specific surface area measurements were determined with a BET method using Sorptomatic 1900 apparatus (Carlo-Erba) with nitrogen as an adsorbate. Prior to the measurement, all samples were degassed for 4 h at 250°C. The specific surface area S_{BET} was calculated using BET equation.

Atomic Absorption Spectroscopy (AAS) analyses were performed with a Solaar M6 Unicam spectrophotometer in order to estimate the amount of Au deposited on support, as described previously [9, 10].

High Resolution Transmission Electron Microscopy (HRTEM) measurements were carried out using high resolution microscope EM-002B (TOPCON) at 10^{-5} Pa, in order to determine an average Au particle size and to define their distribution, in details described previously [9, 10].

X-ray diffraction (XRD) patterns were obtained at room temperature using a PANalytical X'Pert Pro MPD diffractometer, operating at 40 kV and 30 mA (CuK_α radiation). Data were collected in the range 2θ of 20°–80° with a step size of 0.0167° and step time of 10 s. JCPDS files were used for the identification of the diffraction peaks, as described previously [9, 10].

Hydrogen Temperature Programmed Reduction ($TPR\text{-}H_2$) experiments were carried out by PEAK-4 apparatus equipped with a thermal conductivity detector (TCD). $TPR\text{-}H_2$ experiments were performed using a H_2/He gas mixture (5 vol % H_2, 95 vol % He), with a flow rate of 40 cm^3/min, in the temperature range 25–850°C, with a ramp rate 15°C/min.

Powdered samples of 100 mg were exposed to dry Ar at 250°C for 1 h before the reduction. Based on the H_2 consumption, reduction degrees of the investigated samples were calculated. The reduction of NiO to metallic Ni, according to the reaction $NiO + H_2 \longrightarrow Ni + H_2O$, as a standard to calibrate the H_2 consumption, was used. As the first step of the calibration, the peak area under the $TPR\text{-}H_2$ profile for NiO reduction was estimated. The obtained value responded to the theoretical quantity of the reducing agent used during the process. For the tested samples, H_2 consumption was estimated using the following equation:

$$H_2\ (\text{mmol/g}) = (S_{oxide}/m_{oxide}) \times (m_{NiO}/S_{NiO}) \times (1000/74.69), \quad (1)$$

where S_{oxide} and S_{NiO} correspond to the peak area under the TPR profile for the investigated sample and NiO, respectively; m_{oxide} and m_{NiO} correspond to the studied and NiO sample weight, respectively; 74.69 is NiO molar weight (g/mol).

CO oxidation reaction was carried out at atmospheric pressure in a quartz flow microreactor containing 100 mg of sample in a fixed bed, using a series of mass flow controllers with diluted gases. The gas mixture containing 1.6 vol % CO and 3.3 vol % O_2 (He as an eluant gas) was used with a flow of 50 cm^3/min, in the temperature range 25–300°C (for the catalysts) and 25–550°C (for the oxide supports), with a ramp rate 5°C/min. Gas chromatograph fitted with molecular sieves 5 Å, equipped with TCD was used to perform the analysis of both CO and O_2 concentration [9, 10]. The CO conversion was calculated, as described previously [16]. The catalytic activity was assessed in terms of T_{10}, T_{50}, and T_{100}, defined as the temperature at which 10, 50, and 100% CO conversion was obtained, respectively.

The model developed by Johnson and Mooi [13] is based on the qualitative relationship between the amount of the capping oxygen and BET surface area. For this model, the authors considered that the reduction of CeO_2 corresponds to the elimination of one fourth of the surface oxygen ions and each ceria crystallite is a cube of n oxygen ions on a side. Therefore, each ceria crystallite contains n^3 oxygen ions and $1/2n^3$ Ce ions. Since the number of capping oxygen ions in a crystallite is $O_c = n^3 - (n-2)^3 = 6n^2 - 12n + 8$ and the number of H atoms to reduce half of the O_c ions is $H_c = 2O_c$, the ratio of hydrogen atoms in the capping peak to the total cerium atoms (H_c/Ce) will be: $H_c/Ce = 4(6n^2 - 12n + 8)/n^3$ [13].

RESULTS AND DISCUSSION

BET data show that the specific surface area of all catalysts is slightly lower or comparable to that of a given support oxide (table).

The AAS analysis shows that the real amount of gold deposited on the oxide supports is ca. 15% lower

Characterization data of $Au/CeO_2–ZrO_2$ catalysts and their oxide supports obtained using various physicochemical techniques

Support or catalyst	D, nm (XRD)	S_{BET}, m^2/g	Real Au loading, wt % (AAS)	Total H_2 consumption, mmol/g (TPR-H_2)	(O_c/Ce), %	Activity*		
						T_{10}	T_{50}	T_{100}
$Ce_{0.75}Zr_{0.25}O_2$	7.0 Ce(111)	50.1	–	1.53	29.7	265	340	405
$Ce_{0.5}Zr_{0.5}O_2$	6.4 Ce(101)	46.5	–	1.47	20.7	280	355	415
$Ce_{0.25}Zr_{0.75}O_2$	6.7 Ce(101)	47.9	–	0.85	17.3	300	380	455
$Au/Ce_{0.75}Zr_{0.25}O_2$	7.2 Ce(111)	49.5	1.68	0.95	47.2	5	35	65
$Au/Ce_{0.5}Zr_{0.5}O_2$	6.7 Ce(101)	45.0	1.74	0.87	33.9	50	95	125
$Au/Ce_{0.25}Zr_{0.75}O_2$	7.0 Ce(101)	40.7	1.71	0.66	22.1	60	105	135

* Reaction conditions: $CO : O_2 : He = 1.7 : 3.4 : 94.9$ (vol %); $W/F = 0.12$ g s cm^{-3}.

than the nominal Au loading (2 wt %) (table). According to our previous studies [9], the observed loss of Au is attributed to the removal of non-attached gold complexes, simply adsorbed on the support surface due to the deficient quantity of hydroxyl groups available for anionic exchange, which takes place during the washing step. Moreover, it is known that Cl^- ligands are replaced with OH groups in the exchange species during the ammonia washing [17].

The XRD studies of $Au/CeO_2–ZrO_2$ catalysts showed that at high CeO_2 concentration (75 mol %) in the support, a single cubic phase, fluorite-type structure (JCPDS: 03-065-2975) was favoured, whereas both for intermediate (50 mol %) and ZrO_2-rich (75 mol %) composition, tetragonal one (JCPDS: 03-050-1089) was preferential, similarly to the oxide supports [9, 10]. A shift of main diffraction peaks, corresponding to both face-centered cubic and tetragonal cell (Fig. 1), towards lower 2θ angles was observed, due to the formation of Ce^{3+} cations, having a bigger radius than Ce^{4+} (1.14 Å vs. 0.97 Å) [9, 10]. It suggests the "autoreduction" of the catalysts during the calcination process. The "autoreduction" phenomenon can be also the reason for the change in the catalysts color during drying and calcination processes from yellow to dark grey and from dark grey to graphite, respectively. In general, Au deposition does not have an influence on the crystallite size of the supports. No clear Au reflections were observed in the XRD patterns of all studied catalysts (washed with ammonia solution), suggesting the presence of well dispersed small Au particles (Fig. 1).

The HRTEM studies confirmed the presence of small Au particles in the range of 1–5 nm (approximately 80% of Au particles), with the mean particle diameter of ca. 4 ± 2.0 nm.

The reduction of $Ce_{0.75}Zr_{0.25}O_2$ mixed oxide occurs in one stage with the maximum at 565°C (Fig. 2a). One can see a slight shift of the maximum of the reduction peak towards higher temperature with the increase in Zr/Ce molar ratio. This special behavior could be related to the phase distortion, which would alternatively shorten or lengthen the metal-oxygen bonds. Furthermore, the lengthening of the metal-oxygen bond would result in a lower barrier of energy for the oxygen migration in the bulk [18]. For $CeO_2–ZrO_2$ mixed oxides, especially with the Zr/Ce molar ratio 1 and 3, besides the low temperature reduction peak, a characteristic shoulder in the temperature range 310–510°C is observed. It indicates the existence of at least two types of Ce^{4+} located at different chemical environment, assigned to the reduction of surface or subsurface Ce^{4+}. The deposition of Au on $CeO_2–ZrO_2$ mixed oxides leads to a significant shift of the reduction peak towards lower temperature (Fig. 2b). It suggests that the presence of Au nanoparticles facilitates activation (dissociation) of a hydrogen molecule. Next, the dissociated hydrogen species can migrate by a spill-over process from the surface of the Au particles to the support. The amount of H_2 consumed for the reduction of different samples increases with a decrease in Zr/Ce molar ratio (table). However it should be noted that the amount of H_2 consumed during the reduction of the studied catalysts is lower

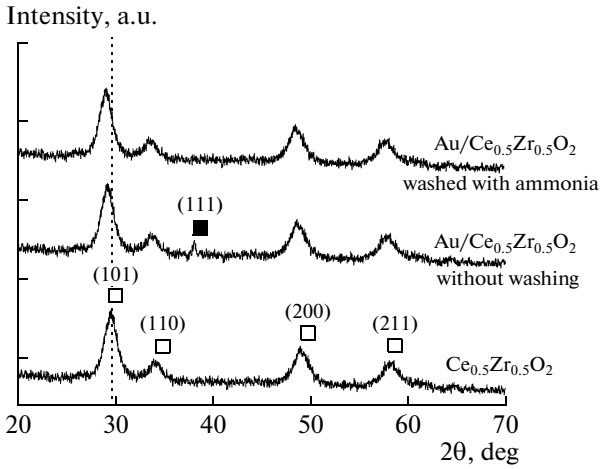

Fig. 1. X-ray diffraction patterns of $Ce_{0.5}Zr_{0.5}O_2$ oxide and $Au/Ce_{0.5}Zr_{0.5}O_2$ catalysts: □—tetragonal-type structure (*P*42/*nmc*) of $Ce_{0.5}Zr_{0.5}O_2$; ■—cubic-type structure (*Fm*3*m*) of Au.

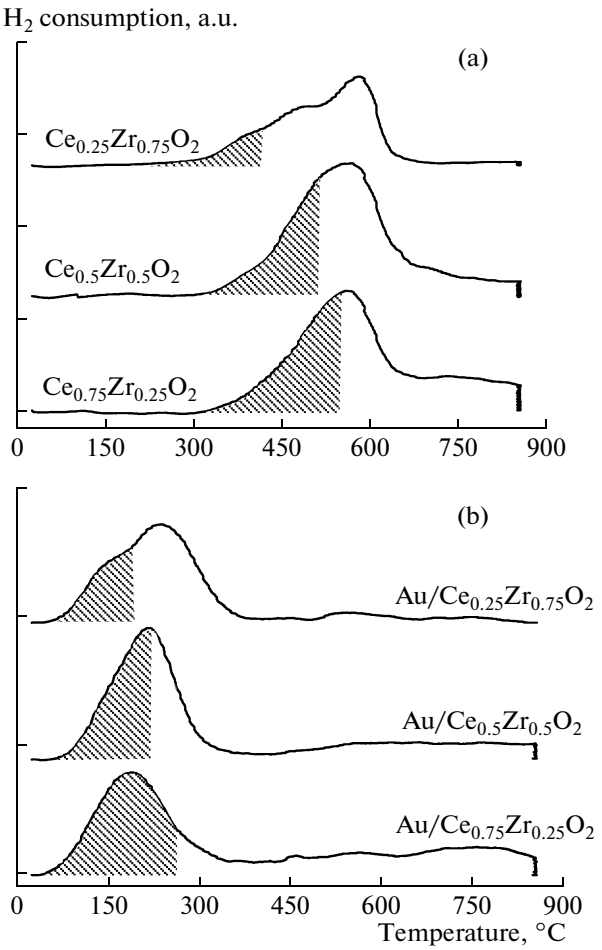

Fig. 2. TPR-H_2 profiles and H_2 consumption for surface reduction according to the Johnson and Mooi model [13] (shadow area): (a) oxide supports, (b) supported Au catalysts. Complementary data see in table.

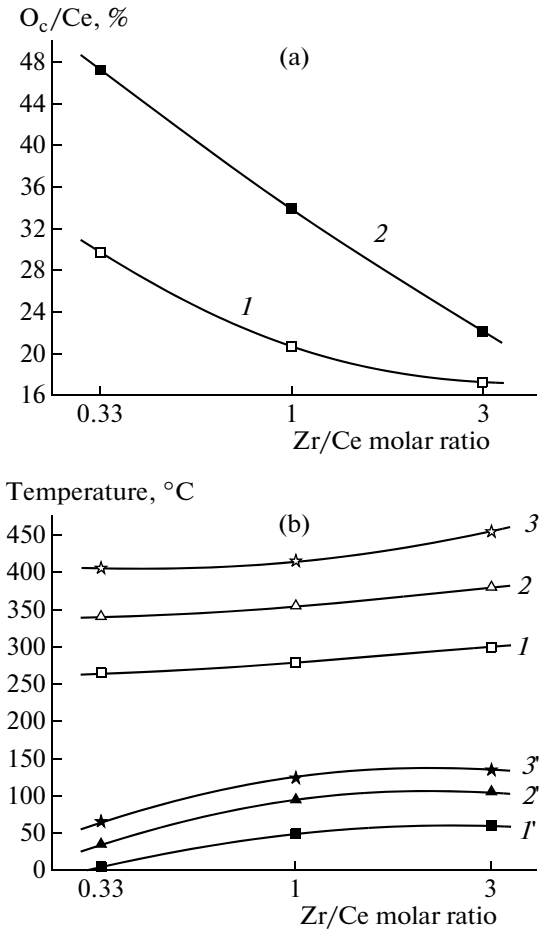

Fig. 3. (a) The effect of Zr/Ce molar ratio on the percentage of oxygen atoms in the capping peak to the total cerium atoms: *1*—oxide support, *2*—supported Au catalyst. (b) The effect of Zr/Ce molar ratio on the activity of the studied solids in CO oxidation on oxide support (*1*–*3*) and supported Au catalyst (*1'*–*3'*): *1*, *1'*—T_{10}, *2*, *2'*—T_{50}, *3*, *3'*—T_{100}. Complementary data see in table.

than that observed for the oxide supports. Additionally, a shift of the four main diffraction peaks, corresponding to the typical oxide-support reflections towards lower 2θ angles was observed. Considering that washing of the Au catalysts with ammonia allows removing residual chlorine [4], which is known to inhibit the reducibility of Ce-containing oxides [18], the catalysts autoreduction during the calcination can occur, as we mentioned above.

It is difficult to quantify the contribution of H_2 consumption for surface and bulk reduction, both for CeO_2–ZrO_2 mixed oxides and Au/CeO_2–ZrO_2 catalysts. Applying the model developed by Johnson and Mooi [13] an approximate evaluation of the H_2 consumption for surface reduction was estimated and is presented as the shaded area under TPR-H_2 curves in Fig. 2. For CeO_2–ZrO_2 oxides, H_2 consumption for the removal of surface oxygen is related to the initial part of the reduction peaks (Fig. 2a). It suggests that the removal of O_2 from bulk of mixed oxides takes place also at low temperature. Moreover, the temperature of the bulk oxygen removal decreases as the Zr^{4+} content increases due to the higher concentration of defects in the fluorite structure of CeO_2, resulting in an increasing oxygen mobility. In the presence of Au nanoparticles, the temperature at which the surface capping oxygen can be removed is significantly lower than that observed for oxide supports (Fig. 2b). Moreover, the percentage of oxygen atoms in the capping peak to the total cerium atoms (O_c/Ce) is much higher than that for the oxide supports (Fig. 3a). It suggests that Au nanoparticles can act like a "pump", assisting in the surface and subsurface oxygen migration, and promoting the reduction of Ce^{4+} to Ce^{3+}. The sequence of the O_c/Ce increasing follows the sequence of the decreasing Zr/Ce molar ratio, both for CeO_2–ZrO_2 oxide supports and Au/CeO_2–ZrO_2 catalysts (Fig. 3a). Furthermore, the activity of both CeO_2–ZrO_2 oxide supports and Au/CeO_2–ZrO_2 catalysts increases with the decrease in Zr/Ce molar ratio

(Fig. 3b). It should be also noted that in the presence of Au nanoparticles the characteristic reduction peaks of oxide supports are shifted towards lower temperature. The most important difference among the analyzed catalysts lies in the extent of this temperature shift which increases with the decrease in Zr/Ce molar ratio in the oxide support, even if similar Au loading was present. It suggests that Au-support interactions are stronger in the case of Au supported on Ce-rich oxide. It confirms the effect of the support composition on the Au-support interactions and its role in the creation of the activity of $Au/CeO_2–ZrO_2$ catalysts in CO oxidation.

For the studied $Au/CeO_2–ZrO_2$ catalysts the sequence of decreasing temperature of the maximum reduction peak clearly follows the sequence of increasing activity (Figs. 2b, 3b). It suggests that the support may provide centres for oxygen activation in form of the oxygen vacancies and for their creation supports redox properties are essential. Moreover, some reduction of the catalyst (i.e. formation of oxygen vacancies) may occur in the reaction mixture. It is generally recognized that in the oxidation reactions the catalyst surface may be partially reduced, adapting itself to the redox potential of the reducing agent/oxygen mixture [8]. Consequently, the higher reducibility of the catalyst is observed (more oxygen vacancies are formed and available at low temperature), the higher activity of the system can be expected (more sites for O_2 activation). It should be also noted that in the case of Ce–Zr mixed oxides no CO conversion at temperatures below 250°C was observed (Fig. 3b). However, in the presence of well dispersed Au their catalytic performance is greatly improved. Considering that the adsorption of CO can occur on both different Au species (Au^{3+}, Au^{+}, and Au^{0}) and CeO_2 [19], the synergetic effect between the support and gold particles at the interface can be suggested.

So, Au nanoparticles supported on $CeO_2–ZrO_2$ mixed oxides with different Zr/Ce molar ratio were characterized with different structural, morphological and catalytic properties. Their activity strongly depends on the support composition and increases with the decrease in Zr/Ce molar ratio. The sequence of the increasing percentage of oxygen atoms in the capping peak to the total cerium atoms (O_c/Ce) follows the sequence of the decreasing Zr/Ce molar ratio in the oxide support. The effect of the support composition on the Au-support interactions and its role in the creation of the activity of $Au/CeO_2–ZrO_2$ catalysts in CO oxidation was confirmed.

REFERENCES

1. Heck, R.M. and Farrauto, R.J., *Catalytic Air Pollution Control*, New York: Wiley, 2002, 2nd ed.
2. Hashmi, A.S.K. and Hutchings, G.J., *Angew. Chem., Int. Ed. Engl.*, 2006, vol. 45, no. 1, p. 7896.
3. Bond, G.C. and Thompson, D.T., *Cat. Rev. Sci. Eng.*, 1999, vol. 41, nos. 3–4, p. 319.
4. Dobrosz, I., Jiratova, K., Pitchon, V., and Rynkowski, J.M., *J. Mol. Catal. A: Chem.*, 2005, vol. 234, nos. 1–2, p. 187.
5. Canaletto, M.P., Longo, A., Venezia, A.M., Martorana, A., and Prestianni, A., *Appl. Catal., A*, 2006, vol. 302, no. 2, p. 309.
6. Ma, Z., Overbury, S.H., and Dai, S., *J. Mol. Catal. A: Chem.*, 2007, vol. 273, nos. 1–2, p. 186.
7. Schubert, M.M., Hackenberg, S., van Veen, A.C., Muhler, M., Plzak, V., and Behm, R.J., *J. Catal.*, 2001, vol. 197, no. 1, p. 113.
8. Grzybowska-Świerkosz, B., *Catal. Today*, 2006, vol. 112, nos. 1-4, p. 3.
9. Dobrosz-Gómez, I., Kocemba, I., and Rynkowski, J.M., *Appl. Catal., B*, 2008, vol. 83, nos. 3–4, p. 240.
10. Dobrosz-Gómez, I., Kocemba, I., and Rynkowski, J.M., *Appl. Catal., B*, 2009, vol. 88, nos. 1–2, p. 83.
11. Dobrosz-Gómez, I., Kocemba, I., and Rynkowski, J.M., *Catal. Lett.*, 2009, vol. 128, nos. 3–4, p. 297.
12. Dobrosz-Gómez, I., Gómez-García, M.A., and Rynkowski, J.M., *Pol. J. Environ. Stud.*, 2009, vol. 18, no. 4, p. 587.
13. Johnson, M.F.L. and Mooi, J., *J. Catal.*, 1987, vol. 103, no. 1, p. 502.
14. Ivanova, S., Petit, C., and Pitchon, V., *Appl. Catal., A*, 2004, vol. 267, nos. 1–2, p. 191.
15. Dobrosz, I., Kocemba, I., and Rynkowski, J.M., *Pol. J. Environ. Stud.*, 2006, vol. 15, no. 6A, p. 32.
16. Dobrosz, I., Gómez-García, M.A., Kocemba, I., Maniukiewicz, W., and Rynkowski, J.M., *Pol. J. Environ. Stud.*, 2005, vol. 14, no. 4, p. 231.
17. Ivanova, S., Pitchon, V., Zimmermann, Y., and Petit, C., *Appl. Catal., A*, 2006, vol. 298, nos. 1–2, p. 57.
18. *Catalysis by Ceria and Related Materials*, Trovarelli, A., Ed., London: Imperial College Press, 2002.
19. Guzman, J., Carretin, S., and Corma, A., *J. Am. Chem. Soc.*, 2005, vol. 127, no. 10, p. 3286.